Time-resolved investigation of subnanosecond radiation from Al wire hybrid *X* pinches

T. A. Shelkovenko,[1] S. A. Pikuz,[1] I. N. Tilikin,[1] A. Elshafiey,[2] and D. A. Hammer[2]
[1]*P. N. Lebedev Physical Institute, Moscow 119991, Russia*
[2]*Cornell University, Ithaca, New York 14853, USA*

(Received 18 September 2020; accepted 30 November 2020; published 17 December 2020)

K-shell x-ray spectra from Al wire hybrid *X* pinches have been studied using an x-ray streak camera with better than 0.1-ns time resolution together with a Focusing Spectrograph with Spatial Resolution (FSSR) spectrograph. High-intensity radiation with a continuumlike spectrum was observed in the subnanosecond initial phase of the x-ray pulse generated by the hybrid *X* pinch (HXP). The absence of spectral lines in this phase and the extremely small x-ray source size indicates the importance of radiative processes in the final phase implosion dynamics. Plasma parameters in the following phases of the HXP were determined from analysis of the line intensities. Point-projection radiography together with a slit-step wedge camera and an FSSR spectrograph without time resolution were used to show the number of radiation sources, and to give information on the time-integrated photon energy spectrum.

DOI: 10.1103/PhysRevE.102.063208

I. INTRODUCTION

Mechanisms generally thought to be responsible for the generation of micropinches that emit short x-ray bursts in high-current *Z*-pinch plasmas are azimuthally symmetric "sausage" instabilities and radiative collapse [1–3]. The sausage instability is a magnetohydrodynamic instability that produces localized pinching of a current-carrying plasma to small radius. Radiative collapse occurs when the current is sufficiently high in a *Z*-pinch equilibrium that the radiative cooling rate exceeds the Ohmic heating rate. The radiative cooling leads to a pinching of the plasma to smaller radius, which increases the radiation rate because the density increases, further increasing the radiative cooling rate of the plasma and enabling it to implode to smaller radius even faster. This process will cease when the plasma becomes so dense that it is optically thick to its own soft x-ray emission, at which time the plasma heats up rapidly, can no longer be confined by the magnetic field, and explodes [4,5].

To study pinching plasmas, including the process of radiative collapse, it is necessary to use a complex diagnostic suite with 10 ps or even better temporal resolution and $\sim$1-μm spatial resolution. Analysis of the detailed properties of micropinch soft x-ray radiation allows us to draw conclusions about the plasma density, ionization state, temperature, and the x-ray source size of micropinches, as well as the number if there is more than one soft x-ray burst. To use a high-resolution diagnostic suite, it must be accurately synchronized with the timing of a micropinch, and it must be looking precisely at the location of the micropinch. One method for reliably creating a micropinch plasma at a predetermined location within $\sim$1 mm to facilitate high-resolution diagnostics is to use an *X*-pinch configuration [4–6]. Standard *X*-pinch plasmas are created using two or more fine wires arranged so that they cross and touch at a single point (forming an "*X*" shape with two wires), with the wires placed as the load of a high-current (>100-kA) pulsed power generator.

A variant of the *X* pinch that involves a single wire connecting two conical electrodes, called the hybrid *X* pinch (HXP), has been developed that produces tiny, localized hot spots and intense continuum x-ray burst like the standard *X* pinch does, but is considerably easier to use [7–9]. By using an interelectrode gap of $\leqslant$2 mm and a wire size that depends upon the pulsed current magnitude and waveform, the HXP can produce micropinches reproducibly at a predetermined location (within $\sim$1 mm) and at a time that can be within $\pm$2 ns of a specific time in the current waveform more than 50% of the time. This enables the concentration of diagnostics at exactly the right place to study the micropinch radiation in detail, including using x-ray-sensitive streak cameras to record x-ray spectra and source size as a function of time.

Micropinches can have different x-ray radiation characteristics and inferred parameters of the plasma responsible for it. There are two terms often used to specify radiating micropinches in *X* pinches: bright spots (BS) and hot spots (HS) [10–12]. Both BS and HS have high temperature ($\sim$1000 eV for Al); the bright spot is a larger diameter radiation source ($\geqslant$10 μm vs $\sim$1 μm in HS) and less dense ($<1021/\mathrm{cm}^3$ vs more than $1021/\mathrm{cm}^3$ electron density in HS) than the hot spot. These differences certainly affect the spectral characteristics of the radiation, which are central to the studies presented in this paper.

The parameters of micropinches in standard *X* pinches were studied in detail in the 2000s using x-ray streak cameras [13–16]. The results we report here are studies of the dynamics of HXPs using an x-ray streak camera for spectroscopic determination of plasma properties and using a suite of time-dependent and time-integrated imaging diagnostics. Aluminum wires were chosen for the first series of experiments because, as shown by experiments with standard *X* pinches

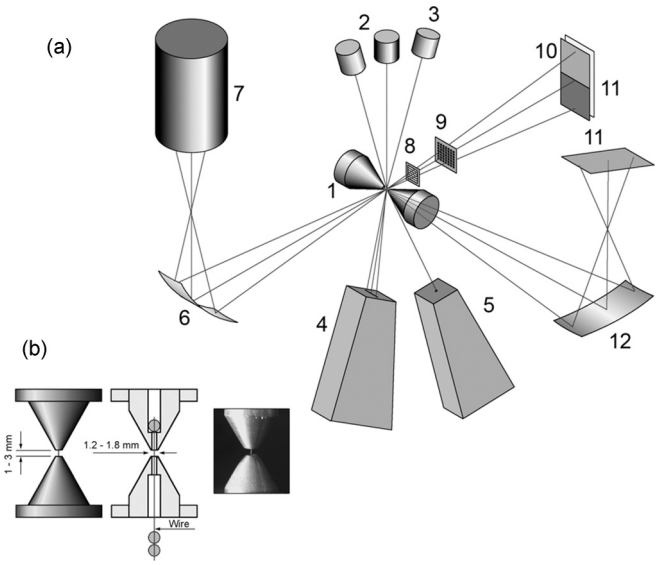

FIG. 1. (a) Schematic drawing of the experimental arrangement for recording HXP radiation: (1) HXP, (2) PCDs, (3) XRD, (4) time-integrated SSW camera, (5) time-integrated x-ray pinhole camera, (6) crystal, (7) streak camera, (8, 9) imaging objects, (10) filters, (11) image plates, and (12) crystal for time-integrated FSSR spectrograph. (b) Hybrid *X* pinch with conical electrodes and its cross section.

[4,13], intense line and continuum radiation can be produced reliably and the soft x-ray bursts last longer ($\geqslant$1 ns) than do the x-ray bursts from other wire materials such as Ti and Mo [13,14]. Therefore, the highest time resolution is not required for the study of Al *X* pinches.

II. EXPERIMENT ARRANGEMENT AND DIAGNOSTICS

The main diagnostic in these experiments was time-resolved spectroscopy. A low trigger-delay Kentech x-ray streak camera with a Focusing Spectrograph with Spatial Resolution (FSSR) was used to record HXP spectra in a slit-free scheme similar to that described in Refs. [13,17]. The experimental arrangement is shown in Fig. 1. The streak camera was specially designed for *X*-pinch experiments and allows recording spectra with streak times ranging from 1 ns for the full 40-mm screen to 90 ns for the full screen. To ensure stability of the camera timing, it was triggered for the present experiments by a signal from an x-ray diffraction (XRD) detector without a filter. The sharp rise time of this signal corresponded to the moment of appearance of HXP UV radiation at the initial breakdown of the wire load about 15–20 ns after the start of the current pulse. From that moment, 25–50 ns remained before the formation of x-ray radiation from the HXP. In order to enable the streak camera's streak-unit voltage pulse to begin quickly enough, the streak unit was located close to the deflecting plates directly on the camera body, which is not the case in a standard x-ray streak camera. The absence of connecting wires from the streak unit to the camera also provided protection against noise, and the camera did not require special shielding. The streak camera provides the ability to record the streak-unit ramp voltage in order to obtain accurate timing if its start is relative to the current pulse

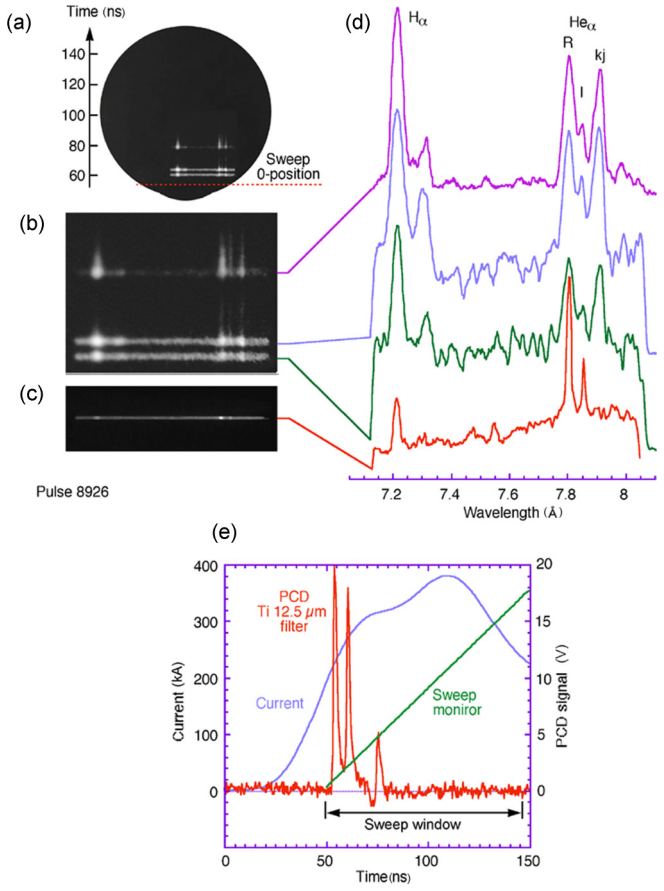

FIG. 2. Results obtained with a 66-μm-diameter Al wire HXP: (a) spectrum recorded on a sweep 2 (see Table I); (b) enlarged part of the image in (a) with the spectra from three x-ray bursts; (c) time-integrated spectrum recorded by an FSSR spectrometer with a mica crystal in the same shot; (d) spectral profiles of all x-ray bursts shown in part (a) and (c); (e) signal from the PCD with a Ti filter is shown together with the load current waveform and sweep monitor signal. [Shot 8926].

and the x-ray burst signals recorded using photoconducting diodes (PCDs), as shown in Fig. 2.

In most of the streak experiments, the camera was used in "sync" mode, in which the beginning of the streaked spectroscopic image is located at the edge of the screen. This mode makes it easier to compare images on the streak camera screen with oscilloscope signals and identify x-ray bursts from the HXP. This configuration of the streak camera allowed the first burst of radiation to be recorded in each shot. However, the price for this simplification is the non-linearity of the initial sweep area, which is especially important for "fast" sweeps. The sweep durations were calibrated based on signals from PCDs recorded by a Tektronix TDS640 oscilloscope. The entire recording path made it possible to reliably record x-ray signals with a time resolution of about 0.5 ns. The streak camera was calibrated using the scan voltage monitor and the PCD signals. The values of average sweep speeds and time resolution values are shown in Table I.

In this series of experiments, a spherically bent quartz crystal with orientation 1010 ($2d = 8.507$ A) with a radius of curvature of 180 mm was used with a streak camera. The

TABLE I. Sweep durations and resolutions.

Sweep	II	III	IV	V	VI
Duration (ns)	90	24	9	3	1
Resolution (ps)	3600	96	36	12	4

peculiarity of quartz is the reflection of radiation mainly in the first order, in contrast to mica, which has multiple efficient reflection orders [15,18]. Reflection in multiple orders creates difficulties in interpreting spectra containing a significant portion of continuum, which is especially important when studying x-ray spectra from *X*-pinches micropinches. For example, when registering the *K*-shell spectrum of aluminum in the second order of reflection of mica (wavelength range 5.2–8.2 A), radiation in the third order (3.47–5.47 A), the fifth order (2.08–3.28 A), and higher orders can be recorded simultaneously. If longer wavelength radiation can be significantly attenuated by appropriate filters, then shorter wavelength radiation can be analyzed using the results obtained. Reflection orders from a mica crystal can also be separated using a crossed-dispersion scheme [19], but this would be technically complex in combination with a streak camera, and so such a scheme has not yet been implemented anywhere. Thus, using a quartz crystal with a single dominant reflection order is an important simplification.

Another difficulty in analyzing the time dependence of spectral line intensities is the end to end nonlinearity of the streak camera recording channel: x-ray–photocathode–electron beam–phosphorescent screen (light)–light amplifier–detector (photographic film or digital camera). The most significant sources of nonlinearity are the light amplifier and photographic film. The use of a digital camera for recording the image simplifies the processing of results, but it has a smaller dynamic range than photographic film and is very sensitive to scattered hard radiation from the *X* pinch and the current generator itself. To calibrate images of intensity-based scans of spectra, we used time-integrated images of the same spectra recorded on image plates with high linearity and a large dynamic range [20,21]. Due to the complexity of the calibration procedure (it will be described elsewhere), we can only talk about the linearization of spectra by intensity and for spectra analysis are using only relative intensities. So when analyzing spectra, we have tried to avoid situations where the absolute value of the intensity change is critical to the conclusion to be drawn.

Time-resolved spectroscopy was supplemented with space-resolved, time-integrated spectroscopy (Fig. 1). The spatial resolution was approximately 200–300 μm. In these experiments, a mica crystal was used. A slit-step wedge (SSW) camera [22] was used to determine the number of radiation sources and their energy distribution (Fig. 1). The spatial resolution of the camera was >100 μm, and so high-magnification point-projection radiography was used to more accurately determine the number of x-ray source points and the size and intensity of the HXP radiation sources (Fig. 1). This diagnostic can provide high spatial resolution with field of view limited only by the geometry of the experiment and the film dimensions; therefore, it was possible to study radiating objects with large magnification [4,5,12,23]. The spatial resolution of point-projection radiography in our experiments was determined mainly by the diffraction limit of resolution, which depends on the geometry of the experiment. A 50-μm-thick tantalum plate with 250-μm-diameter drilled holes was used as the object for the image. By reducing the distance between the depicted object and the radiation source, the magnification in the experiments varied from 15 to 69. As the second object, SiC fibers with a thickness of 10–15 μm were used, which are translucent for the Al *K*-shell radiation. Sometimes, instead of fibers, a Ni mesh with 2000 lines per inch was used. The fibers and mesh were placed as close as possible to the radiation source to obtain images with magnification up to 69 and reduce the diffraction limit of resolution to 2 μm.

The experiments reported here were carried out on the XP pulsed-power machine, which delivers a 100-ns rise-time pulse to a current of $\sim$350 kA, as shown in Fig. 2(e).

III. EXPERIMENTAL RESULTS

To study HXPs with Al wires, two spectrograph settings were applied, one for H-like and He-like Al resonance lines, and the second one for shorter wavelength lines, with a setting of 28 ° and 45 °, respectively.

The main goal of experiments with tuning to the Al resonance lines was to try to record *K*-shell resonance line radiation from the HXPs before the continuum radiation. To radiate these lines plasma electron temperature and ion density must be $T_e > 100$ eV, $N_i > 10^{19}$ ions/cm^3, respectively. In all 10 shots with this spectral tuning and with spectra recorded on sweeps 2, 3, and 4, there was no evidence for resonance line radiation before the first burst of continuum radiation. Using sweep 2, Fig. 2(a) shows a complete picture of the spectral dynamics of the HXP and gives an idea of the duration of the longest wavelength lines of He-like Al. The longer-lived lines are visible for about 6 ns, which is slightly shorter than the duration of the same lines in standard Al *X* pinches [13,15].

This example also shows a significant difference in the spectra recorded with and without time resolution. In all three bursts of the spectrum recorded by the streak camera, the intensity of the H-like Al lines appears to be higher than the He-like Al lines. However, when recording radiation using a streak camera, one must take into account the variation in the sensitivity of the photocathode as a function of photon energy [5], as well as the variation in absorption in the photocathode and filters on the radiation path. Taking all these factors into account in our experiments gives a correction factor of about 1.5 to the intensity of the He-like Al lines relative to the H-like lines. When this factor is taken into account, the H- and He-like Al become about the same intensity, which means that the plasma temperature in each burst is relatively high ($400 <$ Te < 600 eV when $10^{21} <$ Ni $< 10^{22}$ cm^{-3} at the source size 20 μm). In the case shown in Fig. 2, the spectrum without resolution in time gives the opposite picture. The resonance line of the He-like Al is almost three times higher in intensity than the resonance line of H-like Al. This cannot be explained by the difference in absorption of the spectrograph filter and a very small difference in the sensitivity of the plates for

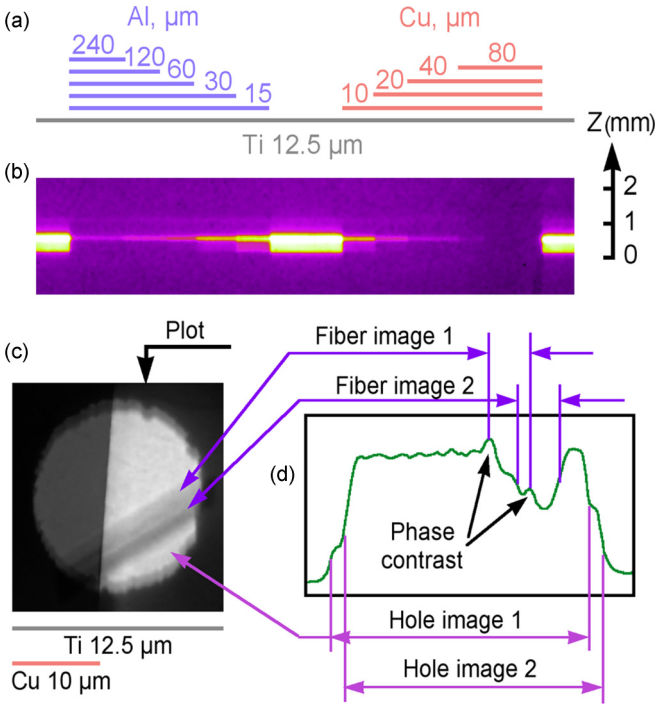

FIG. 3. Imaging diagnostics data for the shot, spectroscopic data from which are shown in Fig 2: (a) filter for SSW camera; (b) SSW image; (c) fragment of point-projection image of a mask with 250-μm diameter hole (29× magnification) and a fiber recorded with 61 times magnification. Filters are shown on the figure. (d) The image profile. Shot 8926.

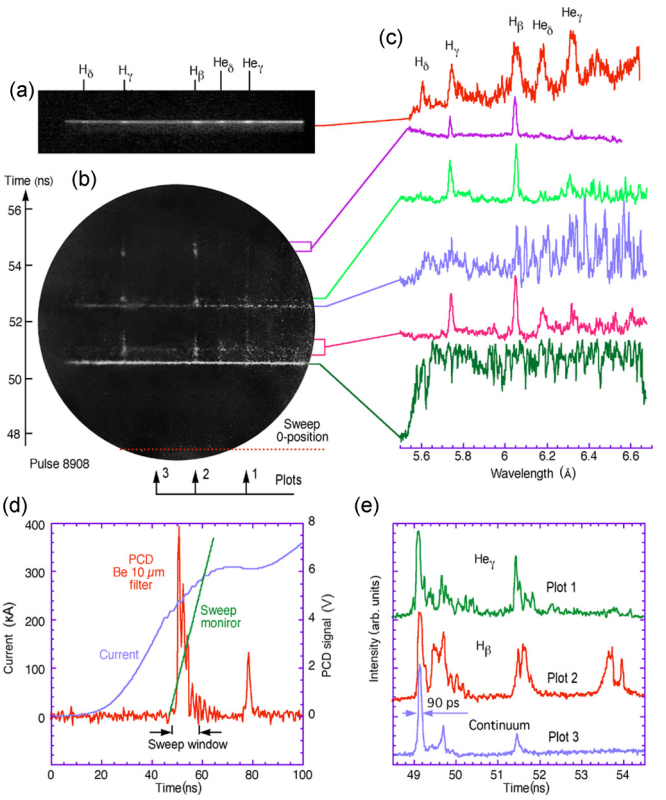

FIG. 4. Results obtained from a 66-μm-diameter Al wire HXP showing: (a) the time-integrated FSSR spectrum and its spectral profile; (b) spectra recorded on a sweep 4 (9 ns for the full screen) with profiles of all bursts; (c) the signal from a PCD with a 10-μm Be filter together with the load current and the sweep monitor signal; (d) and the temporal profiles of Heγ and H$_\beta$ lines and continuum in time. Shot 8908.

different lines [5]. Most likely, this difference is due to significantly different total emission time of H- and He-like Al lines. From this we can conclude that spectra without time resolution can give incorrect results even with a rough estimation of plasma parameters. For the FSSR spectrum registered in shot 8926, the plasma parameters should be as follows: Te $\leqslant$ 300 eV when Ni $\sim 10^{21}$ cm^{-3} at the source size 20 μm.

Using the HXP example shown in Fig. 2, we also can show the importance of a complex suite of diagnostics that includes both subnanosecond resolution time-dependent instrumentation and time-integrated diagnostics for understanding spectral information and *X*-pinch dynamics. The spectrum with time resolution [Fig. 2(a)] shows three bursts of radiation, and two of them are approximately equal based on the intensity of the continuum and line spectra. The third burst is much weaker and almost without continuum radiation. The PCD also shows three x-ray bursts [Fig. 2(e)], with the first and second being almost the same intensity, and the third being much less intense. The time between the first two bursts is 7 ns, and between the second and third burst is 15 ns. In addition, in this shot we also have an image from the SSW camera, which shows a single relatively large source of radiation [Fig. 3(a)] because this instrument was not used in a configuration with a large magnification and high spatial resolution. Only images of test objects recorded with a large magnification and a high spatial resolution can be used to give an accurate number of radiation sources when they are within a millimeter of each other. In Fig. 3(c), one can see two clear images of 250-μm hole in a mask, one of which

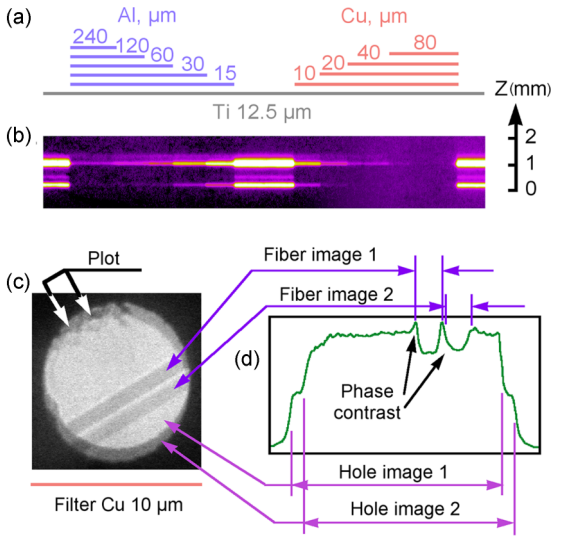

FIG. 5. Filters of SSW camera (a) and SSW image (b); fragment of point-projection image of a 250-μm diameter hole (magnification 29×) and a fiber with 15-μm diameter recorded with 61× magnification through a 10-μm Cu filter; (d) the image profile from the first two x-ray bursts. Shot 8908.

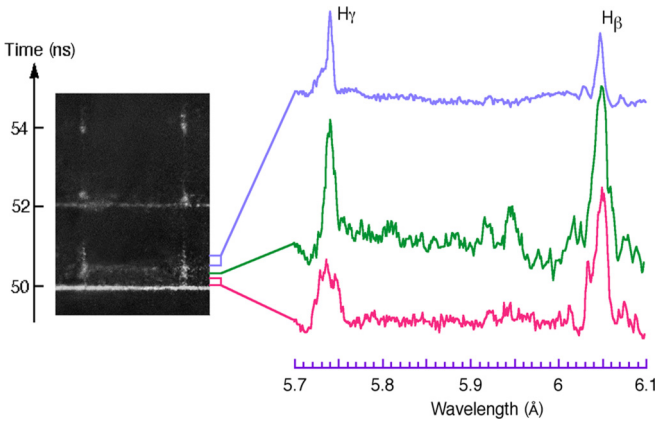

FIG. 6. Spectra recorded in shot 8908 on a sweep 4 are shown magnified with profiles of the first burst showing variation in the linewidth as a function of time.

is shifted relative to the other by 19 μm. In addition, there was also a fiber that was put on the hole that also shows two images. The third burst emits almost no continuum radiation and so no image is registered from it. (The 12.5-μm Ti filter used for the image in Fig. 3(c) cuts off the Al *K*-shell line radiation.) The image profile in Fig. 3(b) shows two images of a fiber, with phase contrast visible in the images and the image profile [Fig. 3(d)]. This indicates that the size of the source in continuum radiation is of the order of 1 μm, which is significantly smaller than the size of the source in spectral lines. This is in good agreement with the source size measurements in standard *X* pinches [6]. According to our previous research [10–12], we can conclude that the first two bursts correspond to criteria of hot spots, small high density X-ray sources, and the third one to a bright spot, a larger, substantially less-dense x-ray source that is incapable of producing a point-projection image of a small object.

The next setting of the streak camera spectrograph and FSSR were for the higher-energy transitions in the He- and H-like Al. These spectra are shown in Figs. 4(a) and 4(b). In this shot, three bursts of radiation were recorded by the PCD in the streak time window, and only in the first two bursts was intense continuum radiation seen. There is no line radiation at all during the first burst as is clear in its spectral profile [lowest (green) spectral profile in Fig. 4(b)]. Against the background of continuum radiation of the second burst, M- and He-like Al lines are observed [second profile from the bottom in Fig. 4(b)].

The SSW camera shows multiple bursts with different emitted energy [Fig. 5(b)]. One x-ray burst which passes only through a Ti filter is not from an extremely dense micropinch. It corresponds in time to the third burst on the sweep spectrum [Fig. 4(b), at about 54.5 ns]. This burst does not have continuum radiation and H-like lines are dominant, which indicates a high plasma temperature [see Fig. 4(b) as well as Figs. 6 and 7(a)]. The other two bursts on the SSW camera have some higher energy radiation, but both bursts are much more intense [Fig. 5(b)]. These two bursts correspond to the first and second burst in the spectrum with time resolution [Fig. 4(b)]. We can conclude that the first two bursts in the time-resolved spectrum are emitted by extreme density and temperature micropinches, or "hot spots." The line radiation from these hot spots in the higher spectral band decays over less than 1 ns (Fig. 4). On sweep 4, the burst duration of continuum radiation appears to be about 80 ps. From the profiles taken during the first burst and shown in an expanded view in Fig. 6, it can be seen that the line radiation in this spectral band becomes most intense about 100 ps after the burst of continuum radiation. Over time, the lines become narrower as the intensity of H-like lines decreases from the maximum-intensity profile (green line) to a lower-intensity profile about 200 ps later (blue line). Figure 7 shows the calculated spectra for different plasma parameters. Comparison of calculated and experimental spectra leads to the conclusion that the plasma density monotonously decreases, and temperature first increases and then decreases. Similar dynamics of the line radiation was observed in other shots (to be discussed shortly).

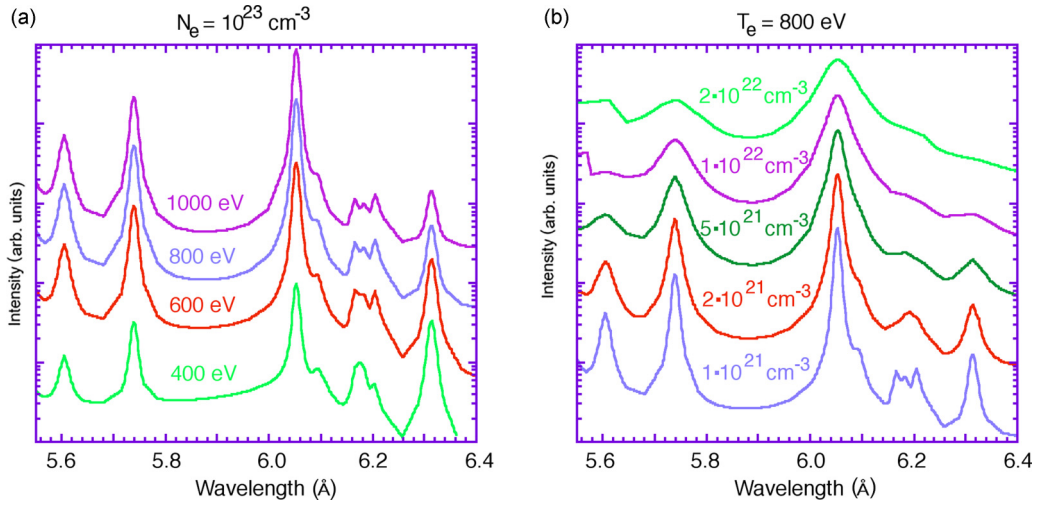

FIG. 7. Calculations of the intensity of the lines made using the PRISM program: (a) the intensity of He-and H- like Al lines depending on the plasma temperature; (b) the linewidth depending on the electron density. The calculations were made at a source size of 20 μm.

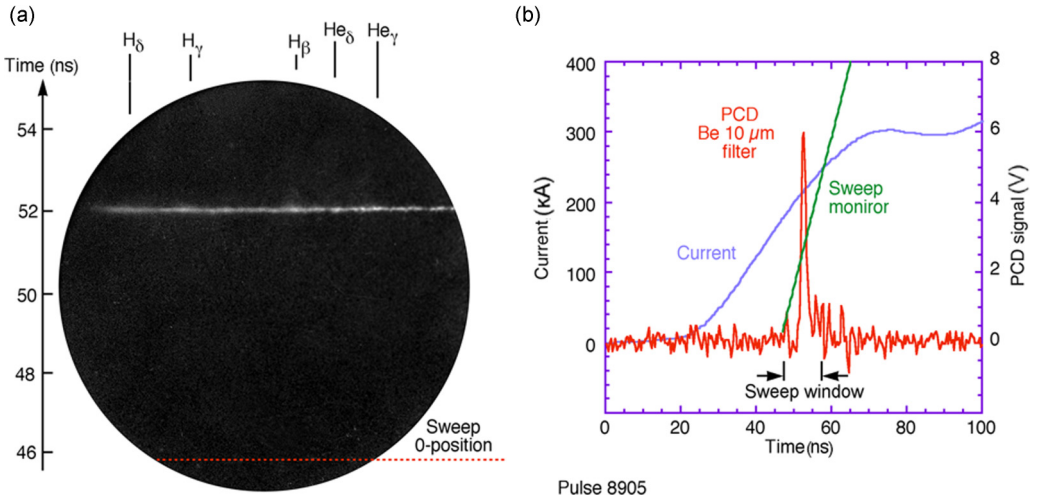

FIG. 8. Results obtained from a 66-μm-diameter Al wire HXP showing: (a) a spectrum recorded on a sweep 4; (b) current and signal from a PCD with a 25-μm Be filter ($E > 1.5$ keV). Shot 8905.

Calculations of the intensity of the lines made using the PRISMSPECT program [24] show that the intensity of H-like lines increases with increasing temperature over the range 400–1000 eV, and the intensity of He-like lines decreases [Fig. 7(a)]. Calculations of the dependence of the intensity and linewidths were also made using the same program for electron temperatures of 400, 600, 800, and 1000 eV. Figure 7(b) shows the calculations for the plasma temperature of 800 eV, which is the best match for the recorded spectra. The PRISMSPECT estimation of the electron temperature using the line radiation is about 600–800 eV and the electron density is about $(2–5) \times 10^{22}$ cm^{-3} in the first burst and goes down to about 10^{20} cm^{-3} in the third one. The radiograph of a test objects shows two images, both with phase contrast, that are shifted about 30 μm relative to each other [Figs. 5(c) and 5(d)]. This confirms the formation of two hot spots in this HXP.

It should be noted that the spectrum shown in Fig. 4 is one of the few spectra with clearly distinguishable Al lines that appear in the time-dependent and time-integrated spectra. Among more than 30 shots with the spectrograph tuned to higher-energy transitions and recorded on sweep 4 or 5, most showed a pulse of continuum radiation without following line radiation as is shown in Fig. 8(a). From Fig. 8(b) one can see that only one burst of radiation was recorded by PCD. The peculiarity of this spectrum is the absence or low intensity of line radiation when the hotspot is decaying.

The spectrum shown in Fig. 9(b) was recorded on sweep 5 with the highest time resolution (Table I) used in these experiments. In this HXP, the spectrum of the first burst of three seen by the PCD shown in Fig. 9(c) is in the streak image [Fig. 9(b)]. Intense continuum radiation and the most intense lines within recorded range are visible until the end of the streak. Duration of the continuum burst is about 70 ps and the most intense part of the line radiation lasts 100–200 ps [Fig. 9(d)]. The FSSR spectrograph also registered intense continuum and a relatively low intensity of line radiation [Fig. 9(a)]. Evidently in this shot, 8911, the duration of the lines in all bursts is lower than in shot 8908 (Fig. 4).

IV. DISCUSSION

From the results obtained, we conclude that the use of spectra without time resolution to calculate plasma parameters will give incorrect results, but rather a lower limit of the parameters of the HXP plasma. Unfortunately, due to the features of the streak camera operation noted above and others (photocathode quality, for example), the time-dependent spec-

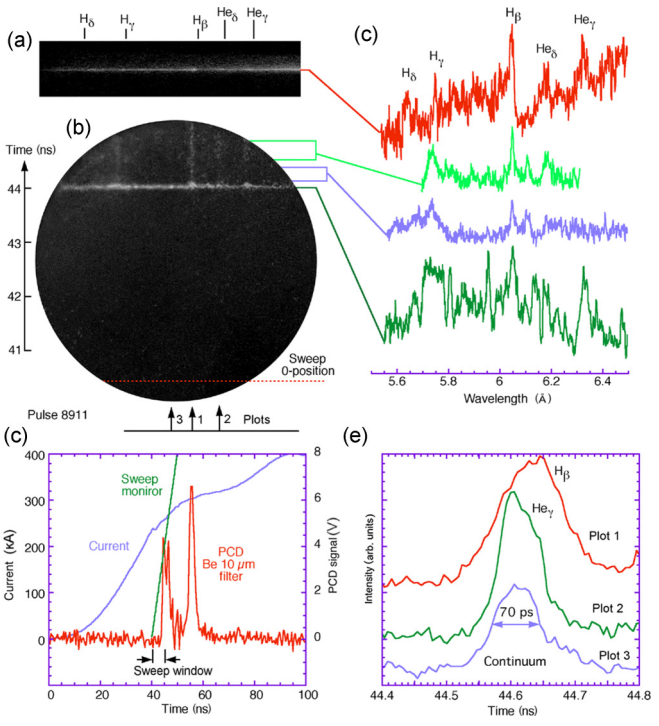

FIG. 9. Results obtained with a 66-μm-diameter Al wire HXP showing: (a) a time-integrated FSSR spectrum with the spectral profile; (b) spectrum recorded on a sweep 5 with profiles of different portions of the recorded x-ray burst; (c) the PCD signal with a Be filter together with the load current and sweep monitor signal; (d) profiles showing intensities of Heγ, H$_\beta$ lines and continuum in time. Shot 8911.

tra are also difficult to use for accurate calculations. Therefore, only estimates of plasma parameters are given in this paper, but they are almost certain to be much more accurate than plasma parameters estimated from time-integrated spectra.

When comparing the radiation dynamics of standard [13] and hybrid *X* pinches with Al wires, the continuum burst is more intense and its duration is much shorter in the HXPs. The appearance of a burst of continuum radiation in the absence of lines, which was not seen in any streak camera images from standard *X* pinches, corresponds to a very high plasma density in the micropinch. Estimations of plasma density also showed that the plasma density in hot spots formed in standard Al wire *X* pinches [13] is about an order of magnitude lower than in Al wire HXPs as found here. According to our calculations for the electron temperature of 400, 600, 800, and 1000 eV, the electron density should be higher than $10^{22}\,\mathrm{cm}^3$ to get only continuous radiation in HXPs with Al wires. The duration of the burst of continuum radiation is about 70–80 ps, and then abruptly disappears, and little or no radiation is observed for 100 ps or longer. Later, secondary pinching may occur with very low plasma parameters, which are not always detected by PCDs. Such dynamics of micropinches in HXPs may indicate their formation through radiative collapse. The few works devoted to radiative collapse [3,25–27] do not contain criteria that can currently be measured experimentally, and so we can claim only that such rapid changes in the parameters of the radiation burst produced by *X* pinches may be an indication of radiative collapse. Similar experiments carried out with Mo and Ti wire HXPs, which are now being prepared for a future publication, do not contradict this possibility.

V. CONCLUSIONS

Experiments have shown that the radiation of all Al wire HXPs begins with a short but intense burst of continuum radiation. In HXPs with a single source of radiation, line radiation is not recorded at high sweep speeds of the streak camera, although spectrographs without time resolution typically record intense line spectra. The duration of bursts of continuum radiation is 70–80 ps, and the duration of the lines can reach 5–7 ns.

The radiation spectra show a significant difference in the dynamics and parameters of the plasma in standard and hybrid *X* pinches with aluminum wires.

ACKNOWLEDGMENTS

This research is supported by the Department of Energy Grant No. DE-SC0018088 as well as by the National Nuclear Security Administration Stewardship Sciences Academic Programs under Department of Energy Cooperative Agreement DE-NA0003764.

[1] R. S. Pease, Equilibrium characteristics of a pinched gas discharge cooled by bremsstrahlung radiation, Proc. Phys. Soc. B **70**, 11 (1957).

[2] S. I. Braginskii, The behavior of a completely ionized plasma in a strong magnetic field, Sov. Phys. JETP **6**, 494 (1958).

[3] K. N. Koshelev and N. R. Pereira, Plasma points and radiative collapse in vacuum sparks, J. Appl. Phys. **69**, R21 (1991).

[4] T. A. Shelkovenko, D. B. Sinars, S. A. Pikuz, and D. A. Hammer, Radiographic and spectroscopic studies of X-pinch plasma implosion dynamics and x-ray burst emission characteristics, Phys. Plasmas **8**, 1305 (2001).

[5] S. A. Pikuz, T. A. Shelkovenko, and D. A. Hammer, X-Pinch Part I, Plasma Phys. Rep. **41**, 291 (2015).

[6] S. A. Pikuz, T. A. Shelkovenko, and D. A. Hammer, X-Pinch, Part II, Plasma Phys. Rep. **41**, 445 (2015).

[7] T. A. Shelkovenko, S. A. Pikuz, A. D. Cahill, P. F. Knapp, D. A. Hammer, D. B. Sinars, I. N. Tilikin, and S. N. Mishin, Hybrid X-pinch with conical electrodes, Phys. Plasmas **17**, 112707 (2010).

[8] T. A. Shelkovenko, S. A. Pikuz, S. A. Mishin, A. R. Mingaleev, I. N. Tilikin, P. F. Knapp, A. D. Cahill, C. L. Hoyt, and D. A. Hammer, Hybrid X-pinches, Plasma Phys. Rep. **38**, 359 (2012).

[9] T. A. Shelkovenko, I. N. Tilikin, G. V. Ivanenkov, W. Stepniewski, A. R. Mingaleev, V. M. Romanova, A. V. Agafonov, A. D. Cahill, C. L. Hoyt, P. A. Gourdain, D. A. Hammer, and S. A. Pikuz, Dynamics of hybrid X-pinches, Plasma Phys. Rep. **41**, 52 (2015).

[10] V. M. Romanova, I. N. Tilikin, T. A. Shelkovenko, A. R. Mingaleev, E. A. Bolkhovitinov, A. A. Rupasov, A. E. Ter-Oganesyan, and S. A. Pikuz, The hybrid X-pinch as a source of XUV radiation, IEEE Trans. Plasma Sci. **46**, 3837 (2018).

[11] R. D. McBride, T. A. Shelkovenko, S. A. Pikuz, D. A. Hammer, J. B. Greenly, B. R. Kusse, J. D. Douglass, P. F. Knapp, K. S. Bell, I. C. Blesener, and D. A. Chalenski, Implosion dynamics and radiation characteristics of wire-array Z pinches on the Cornell Beam Research Accelerator, Phys. Plasmas **16**, 012706 (2009).

[12] T. A. Shelkovenko, S. A. Pikuz, and D. A. HammerA review of projection radiography of plasma and biological objects in X-pinch radiation, Plasma Phys. Rep. **42**, 226 (2016).

[13] D. B. Sinars, S. A. Pikuz, T. A. Shelkovenko, K. M. Chandler, D. A. Hammer, and J. P. Apruzese, Time-resolved spectroscopy of Al,Ti,and Mo X pinch radiation using an X-ray streak camera, J. Quant. Spectrosc. Radiat. Transfer **78**, 61 (2003).

[14] T. A. Shelkovenko, S. A. Pikuz, I. Yu. Skobelev, D. B. Sinars, K. M. Chandler, M. D. Mitchell, and D. A. Hammer, X-pinch plasma condition from time resolved x-ray spectroscopy, Rev. Sci. Instrum. **74**, 1958 (2003).

[15] T. A. Shelkovenko, S. A. Pikuz, D. B. Sinars, K. M. Chandler, and D. A. Hammer, Time resolved spectroscopic measurements of ∼1 keV, dense, subnanosecond X pinch plasma bright spots, Phys. Plasmas **9**, 2165 (2002).

[16] S. B. Hansen, A. S. Shlyaptseva, S. A. Pikuz, T. A. Shelkovenko, D. B. Sinars, K. M. Chandler, and D. A. Hammer, Analysis of L-shell line spectra with 50-ps time resolution from Mo X-pinch plasmas, Phys. Rev. E **70**, 026402 (2004).

[17] S. A. Pikuz, T. A. Shelkovenko, D. B. Sinars, D. A. Hammer, S. V. Lebedev, S. N. Bland, I. Yu. Skobelev, J. A. Abdallah, C. J. Fontes, and H. L. Zhang, Spatial, temporal and

spectral characteristics of an X pinch, J. Quant. Spectrosc. Radiat. Transfer **71**, 581 (2001).

[18] G. Hoelzer, O. Wehrhan, J. Heinisch, E. Foerster, T. A. Pikuz, A. Y. Faenov, S. A. Pikuz, V. M. Romanova, and T. A. Shelkovenko, Flat and spherically bent muscovite (mica) crystals for X-ray spectroscopy, Phys. Scr. **57**, 301 (1998).

[19] S. A. Pikuz, B. M. Song, T. A. Shelkovenko, K. M. Chandler, M. D. Mitchell, and D. A. Hammer, Application of the focusing x-ray spectrograph with crossed dispersion to investigations of X pinch plasmas, Rev. Sci. Instrum. **75**, 3777 (2004).

[20] K. Ren, T. Xu, J. Zheng, J. Dong, M. Wei, C. Li, Z. Cao, and H. Du, Calibration of the linear response range of x-ray imaging plates and their reader based on image grayscale values, Rev. Sci. Instrum. **88**, 083115 (2017).

[21] G. Dunham, E. C. Harding, G. P. Loisel, P. W. Lake, and L. B. Nielsen-Weber, Cross-calibration of Fuji TR image plate and RAR 2492 x-ray film to determine the response of a DITABIS SuperMicron image plate scanner, Rev. Sci. Instrum. **87**, 11E301 (2016).

[22] S. A. Pikuz, T. A. Shelkovenko, D. B. Sinars, and D. A. Hammer, Temporal characteristics of X-ray emission from X-pinches, Plasma Phys. Rep. **32**, 1020 (2006).

[23] T. A. Shelkovenko, D. B. Sinars, S. A. Pikuz, K. M. Chandler, and D. A. Hammer, Point-projection X-ray radiography using an X pinch as the radiation source, Rev. Sci. Instrum. **72**, 667 (2001).

[24] J. J. Macfarlane, I. E. Golovkin, P. R. Woodruff, D. R. Welch, B. V. Oliver, T. A. Melhorn, and R. B. Campbell, *Inertial Fusion Sciences and Applications: State of the Art* edited by B. A. Hammel (IFSA, 2003) p. 457.

[25] M. G. Haines, An analytic model of radiative collapse of a Z-pinch, Plasma Phys. Controlled Fusion **31**, 759 (1989).

[26] V. V. Vikhrev, Constriction of Z-pinch due to radiation losses, JETP Lett. **27**, 95 (1978).

[27] J. P. Chittenden, A. J. Power, and M. G. Haines, Further investigations of radiative collapse in a Z-pinch, Plasma Phys. Controlled Fusion **31**, 1813 (1989).